Journal of Immunological Methods 511 (2022) 113381

Contents lists available at ScienceDirect

Journal of Immunological Methods

journal homepage: www.elsevier.com/locate/jim

Receptor-ligand non-equilibrium kinetics (RLNEK) 1.0: An integrated Trackmate laminar flow chamber analysis

Zachary A. Rollins [b,1], Allison Chan [b,1], Venktesh S. Shirure [a], Steven C. George [a,*]

[a] Department of Biomedical Engineering, University of California, Davis, Davis, CA, USA
[b] Department of Chemical Engineering, University of California, Davis, Davis, CA, USA

ARTICLE INFO

Keywords:
2D kinetics
Surface-tethered reactants
Shear flow
Leukocyte
Transmigration

ABSTRACT

Although parallel plate flow chamber assays are widely performed, extraction of kinetic parameters is limited to specialized labs with mathematical expertise and customized video-microscopy tracking tools. The recent development of Trackmate has increased researcher accessibility to tracking particles in video-microscopy experiments; however, there is a lack of tools that analyze this tracking information. We report a software tool, compatible with Trackmate, that extracts Receptor Ligand Non-Equilibrium Kinetic (RLNEK) parameters from video-microscopy data. This software should be of particular interest to the community of researchers and scientists interrogating the target-specific binding and release of immune cells.

1. Introduction

The parallel plate flow chamber assay is an experimental method that can be used to characterize biophysics of receptor-ligand interactions. In this assay, the cells are flowed over a surface pre-coated with ligands, mimicking the natural events of immune cells and metastasizing cancer cells in the circulation. The parallel plate flow chamber assay has provided novel insights into the mechanosensing properties of numerous types of cancer and immune cells including selectins, T cell receptors, and B cell receptors (Alon et al., 1995; Lawrence et al., 1997; Lou et al., 2006; Robert et al., 2012; Shirure et al., 2015; Limozin et al., 2019). Notably, the fast-paced interactions of circulating cells or migrating tissue resident cells with relatively static receptors are determined by non-equilibrium properties of the receptor-ligand bond.

To characterize non-equilibrium kinetics of receptor-ligand pairs, a theoretical foundation has previously been developed (Cheung and Konstantopoulos, 2011). In this semi-empirical approach, experiments are conducted to find the capture efficiency and bond lifetime. The data obtained are utilized with the theoretical equations to determine intrinsic kinetic parameters. While parallel plate flow chamber assays are widely performed, the data analysis is often limited to finding the number of interacting cells/spheres. A useful tool, Trackmate, was recently developed to track and quantify the number of interacting cells/spheres (Tinevez et al., 2017). However, the extraction of key kinetic parameters from the experimental data is still limited to specialized labs with the appropriate level of mathematical expertise. In an effort to democratize the accessibility of extracting kinetic parameters from the flow chamber, we have integrated the theoretical foundation of the receptor-ligand non-equilibrium kinetics (RLNEK) with Trackmate outputs from ImageJ. The algorithm has been compiled into a Github repository (https://github.com/zrollins/RLNEK) for open, extensible development. Furthermore, we have also created and made available a python package, with a detailed user guide and instruction manual, compatible with Trackmate in ImageJ.

2. Model description

The equation $N_u + m_l \rightleftharpoons N_b$ describes the dynamic equilibrium between surface-tethered reactants in a laminar flow chamber, where N_u is the number of unbound cells/spheres at some time t, m_l is the ligand site density on the surface floor of the flow chamber, and N_b is the cumulative number of cells/spheres bound up to time t (Cheung and Konstantopoulos, 2011). For illustration purposes, the ligand is tethered to

Abbreviations: RLNEK, Receptor Ligand Non-Equilibrium Kinetic; PDB, protein data bank; TRR, trust region reflective; PDMS, polydimethylsiloxane.

* Corresponding author at: Department of Biomedical Engineering, 451 E. Health Sciences Drive, room 2315, University of California, Davis, Davis, CA 95616, USA.
E-mail address: scgeorge@ucdavis.edu (S.C. George).

[1] Authors contributed equally.

https://doi.org/10.1016/j.jim.2022.113381
Received 9 February 2022; Received in revised form 21 October 2022; Accepted 24 October 2022
Available online 27 October 2022

the flow chamber floor and the receptor is tethered to the cells/spheres (Fig. 1A); however, this can be readily inverted. The reaction between surfaces (i.e., 2D) is controlled by two rate constants: the dissociative off-rate k_{off} (s^{-1}) and the effective on-rate $k_+\left(\frac{\mu m^2}{s}\right)$. Thus, the rate of formation of bound cells/spheres to the chamber floor, N_B, is

$$\frac{dN_b}{dt} = k_+(N_u + m_l) - k_{off}N_b \quad (1)$$

The total number of cells/spheres that pass through the chamber up until time t is N_T, where

$$N_T = N_b + N_u \quad (2)$$

2.1. Capture efficiency, $\frac{N_b}{N_T}$

At infinite time, we assume the reaction between tethered surfaces has reached kinetic equilibrium ($dN_b/dt = 0$) and substitute equation (2) into (1) to solve for the ratio of bound to total cells/spheres up until time t (i.e., capture efficiency, $\frac{N_b}{N_T}$).

$$\frac{N_b}{N_T} = \frac{k_+ m_l}{k_+ m_l + k_{off}} \quad (3)$$

Capture efficiency is an empirical parameter describing the ratio $\frac{N_b}{N_T}$. N_T requires velocity filtering such that the only cells/spheres that are included are those that can interact by traveling at a critical distance from the surface floor. This critical distance, d_c, is defined as $d_c = y - a$ where y represents the distance from the center of the cell/sphere to the chamber floor and a represents the cell/sphere radius. The velocity of the cell/sphere traveling at this critical distance is the critical velocity, u_c, and can be approximated by solving the asymptotic formula for a sphere in free motion near a surface

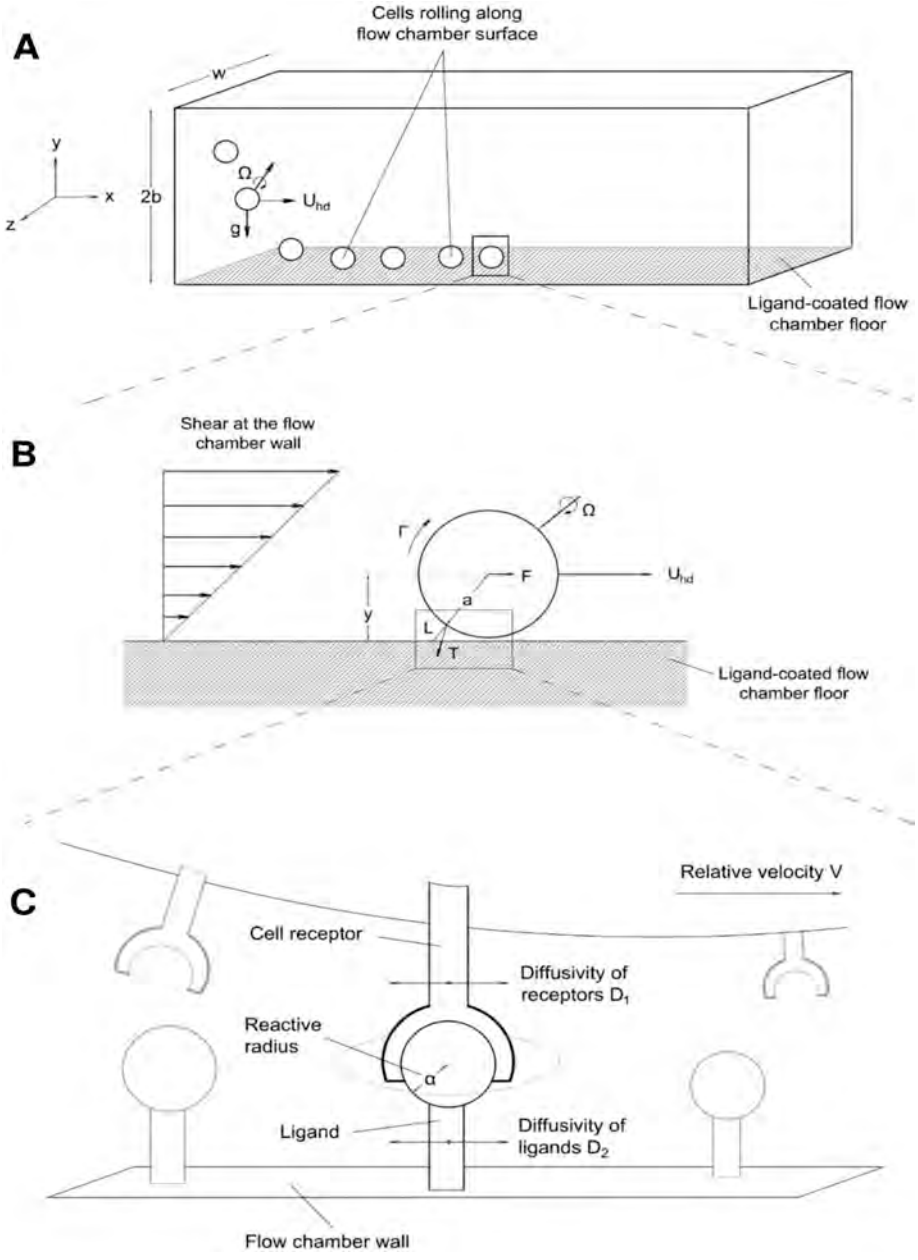

Fig. 1. Levels of Abstraction for 2D Kinetics of Surface Tethered Reactants (A) Millimeter scale of cells/spheres traversing through laminar flow chamber (B) Micrometer scale of cell/sphere interacting with ligand coated flow chamber surface (C) Nanometer scale of the relative motion of the surface tethered reactants.

$$u_c \approx y\gamma_w\left(1-\frac{5}{16}\left(\frac{a}{y}\right)^3\right) \tag{4}$$

where γ_w is the shear rate and $\gamma_w = \frac{\tau}{\mu}$ for a Newtonian fluid (Goldman et al., 1967). The critical distance, d_c, is a user input and the number of tracks with mean velocities, u_{cell}, greater than the critical velocity are excluded from N_T. The mean velocity is the arithmetically averaged instantaneous velocity of cells/spheres over all time frames.

2.2. Estimation of applied tensile force, f

Under laminar flow, hydrodynamic shear acting on a rigid sphere that is tethered to the chamber floor applies a tensile force on the trailing receptor-ligand interaction (Fig. 1B). Hydrodynamic shear at the chamber floor is estimated using the simple Poiseuille model (i.e., pressure driven, infinite cross-sectional aspect ratio).

$$\tau = -\mu\frac{dv_x}{dy}\bigg|_{y=b} = \frac{3\mu Q}{2wb^2} \tag{5}$$

where Q is the volumetric flow rate, μ is the viscosity of the fluid passing through the chamber, w is the flow chamber width, and b is the flow chamber half-height. The hydrodynamic shear of the fluid will impose a hydrodynamic drag force, F, and rotational torque, Γ, on the rigid sphere. As the sphere approaches the chamber floor, shear-induced force and torque approach finite limits, and their extrapolated constants 1.7005 and 0.9440, respectively, are for the limiting case when the sphere touches the wall (i.e., when the cell/sphere is bound to the ligands on the chamber surface (Goldman et al., 1967)),

$$F = 1.7005{*}6\pi\mu a^2\frac{\tau}{\mu} \tag{6}$$

$$\Gamma = 0.9440{*}4\pi\mu a^3\frac{\tau}{\mu} \tag{7}$$

The tensile (or tether) force f is approximated by performing a torque balance on a rigid sphere assumed to be in static equilibrium (Pierres et al., 1995),

$$f \approx \left(F+\frac{\Gamma}{a}\right){*}\sqrt{\frac{a}{2L}} \tag{8}$$

F and Γ are the approximated hydrodynamic drag force and rotational torque, respectively, acting on the sphere and L is the receptor-ligand bond length. Bond length of a receptor-ligand pair may be estimated from crystal structures on the Protein Data Bank (PDB) and molecular visualization software (e.g., Chimera, PyMOL, VMD). The tensile force can be expressed as a function of volumetric flow by combining Eqs. (5)–(8).

$$f = Q\sqrt{\frac{a}{2L}}\left(\frac{1.7005{*}9\pi\mu a^2 + 0.9440{*}6\pi\mu a^2}{wb^2}\right) \tag{9}$$

2.3. Dissociation rate, k_{off}

The dissociation rate for a single receptor-ligand bond, k_{off}, is defined as the inverse bond lifetime. This rate depends on applied tensile force and this dependency determines the dissociation bond behavior. The ubiquitous slip and catch-slip bond dissociation models have been included and can be broadened as needed. The k_{off} dissociation model for a slip bond (Bell, 1980) is,

$$k_{off} = k_{off}^0{*}exp\left(\frac{x_\beta f}{k_bT}\right) \tag{10}$$

where k_{off}^0 is the unstressed dissociation rate, x_β is the reactive compliance, k_b is the Boltzmann constant, and T is the temperature. The two-pathway k_{off} dissociation model for a catch-slip bond (Evans et al., 2004) is,

$$k_{off} = \frac{\varphi_0 k_{1rup} + exp\left(\frac{f}{f_{12}}\right)\left[k_{2rup}exp\left(\frac{x_\beta f}{k_bT}\right)\right]}{\varphi_0 + exp\left(\frac{f}{f_{12}}\right)} \tag{11}$$

where $\varphi_0 = exp\left(\frac{\Delta E_{21}}{k_bT}\right)$. φ_0 is the equilibrium constant between the two states at zero force, k_{1rup} and k_{2rup} are the dissociation rates for pathways 1 and 2, respectively. Pathway 1 corresponds to the region dominated by catch bond behavior, pathway 2 corresponds to the region dominated by slip bond behavior, and f_{12} is the force scale that governs the occupancy ratio of the two states.

2.4. Estimation of $\frac{N_b}{N_T}$ and k_{off}

To characterize the bond dissociation model, k_{off}, and capture efficiency, $\frac{N_b}{N_T}$, the RLNEK user must collect video-microscopy data and accurately track cells/spheres using the Trackmate plugin in ImageJ. A Trackmate guide has been posted in the Github repository to enhance the workflow for RLNEK users to obtain accurate tracks. Given that multi-bond interactions can occur at high site density, surface coating concentrations should be <100 mM to keep adsorbed ligand site density < 100 sites/μm^2. Furthermore, to minimize flow field disturbance, cell/sphere concentrations should be $<0.5 \times 10^6$ cells/mL (Lawrence et al., 1997). Please refer to the *User Guide* for additional details on the set of data files that need to be collected to complete characterization of each module. To accurately track cells/spheres, the user will first mark all cells/spheres for all frames by setting customized parameters and tolerances (e.g., diameter, quality, intensity, contrast, position). These filters allow the user to identify all cells/spheres traveling across the field of view for all frames (Fig. 2A). These cells/spheres are assigned an "ID" with spatiotemporal information outputted in the "spots" output file (Fig. 2B).

After marking all cells/spheres for all time frames, the user will select a tracking algorithm to link the marked cell/sphere "IDs" between frames (e.g., Linear Motion LAP, Simple LAP, Nearest Neighbor Search) (Fig. 3A). The linked "IDs" will be chronologically ordered and distributed into "TRACK_IDs" (Fig. 3B). There will be a singular "TRACK_ID" for each cell/sphere that travels over the field of view. The tracks can be optimized by setting the linking max distance, gap-closing max distance, and gap-closing max frame gap. In addition, the tracks can be adjusted manually to ensure accurate tracking. The output file contains the "TRACK_IDs" and the track mean velocity (u_{cell}) labelled "TRACK_MEAN_SPEED". The tracks (i.e., "TRACK_IDs") are filtered to exclude those with mean velocities, u_{cell}, greater than the critical velocity, u_c. The remaining number of tracks is the total number of cell/spheres that crossed the microscope's field of view (i.e., N_T). A video (Supplementary Video 1) representing cells/spheres attached and flowing across the field of view with projected tracks demonstrates the accuracy and high-throughput capacity of the method.

Next, each track will be evaluated to determine if the cells/spheres satisfy the stopping criteria. For each track, the displacement, is calculated between frames

$$D = \sqrt{(x_t - x_n)^2 + (y_t - y_n)^2} \tag{12}$$

where x and y represent the coordinate position of a cell in a single frame (measured in micrometers), the subscript t represents the current frame, and the subscript n represents the nth previous frame. Time stamped coordinate positions (i.e., x_t, x_n and y_t, y_n) can be obtained from the "spots" Trackmate file under POSITION_X and POSITION_Y, respectively (Fig. 2B). The CCD frames per second is determined from the amount of time between sequential frames. The stopping criteria is satisfied if the cell/sphere displacement D is less than a specified maximum

A

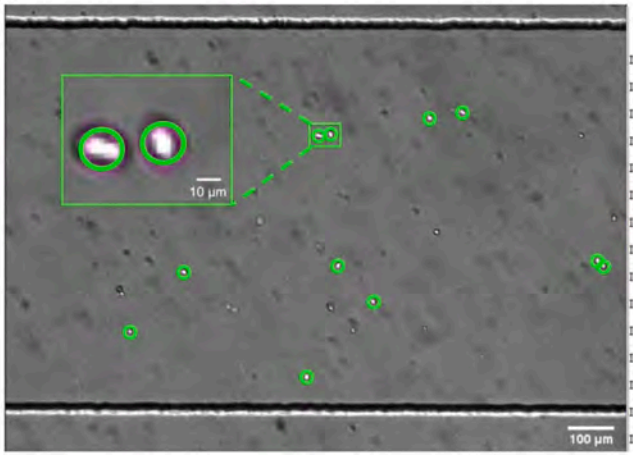

B

Label	Spot ID	Track ID	X (μm)	Y (μm)	Z (μm)	Frame
ID131203	131203	0	978.176	459.904	0	0
ID131216	131216	0	978.191	459.885	0	1
ID131416	131416	0	978.198	459.899	0	2
ID131390	131390	0	978.19	459.92	0	3
ID131164	131164	0	978.178	459.937	0	4
ID131403	131403	0	978.213	459.895	0	5
ID131377	131377	0	978.253	459.807	0	6
ID131256	131256	0	978.261	459.815	0	7
ID131469	131469	0	978.257	459.818	0	8
ID131350	131350	0	978.262	459.838	0	9
ID131429	131429	0	978.232	459.871	0	10
ID131229	131229	0	978.212	459.911	0	11
ID131482	131482	0	978.189	459.949	0	12
ID131549	131549	0	978.162	460.018	0	13
ID131322	131322	0	978.125	460.08	0	14

Fig. 2. (A) Frame of a video depicting spots (or cells) marked in green circles by Trackmate and (B) detailed spatiotemporal information of the marked cells assigned a unique spot ID. The spots are detected for each frame and the spot detection can be optimized in Trackmate utilizing one of the several spot detectors and optimization parameters. The inset is a zoomed in example of the spots detected by Trackmate. (For interpretation of the references to colour in this figure legend, the reader is referred to the web version of this article.)

A

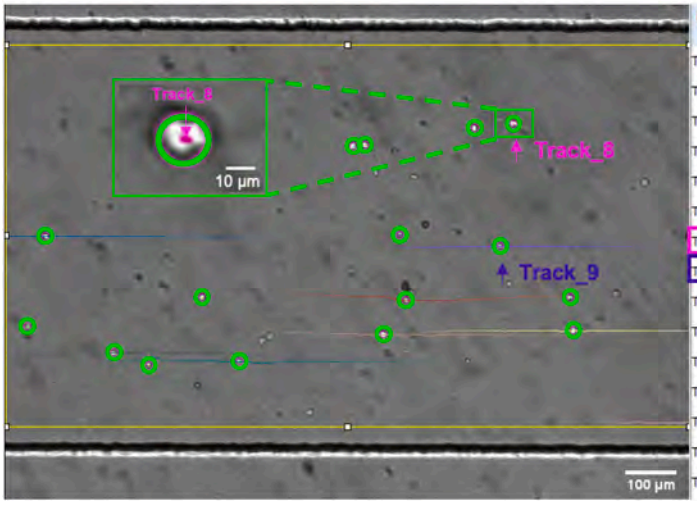

B

Label	Index	ID	N spots	Mean sp. (μm/sec)	Duration (sec)
Track_0	0	0	2400	0.315	299.875
Track_1	1	1	2400	0.287	299.875
Track_2	2	2	2400	0.274	299.875
Track_3	3	3	2400	0.184	299.875
Track_5	5	5	2400	0.285	299.875
Track_7	7	7	847	6.016	106
Track_8	8	8	556	0.592	70.25
Track_9	9	9	369	14.93	46
Track_10	10	10	203	21.41	25.25
Track_39	39	39	345	31.09	43
Track_50	50	50	360	29.727	44.875
Track_51	51	51	841	12.928	105
Track_66	66	66	1828	0.647	228.375
Track_70	70	70	860	0.106	108.375
Track_71	71	71	322	33.189	40.125

Fig. 3. (A) Frame of a video depicting spot (or cell) tracks. Each track colour represents a unique Track ID and the linked spots across frames are displayed by projecting the track 100 frames forward and backward in time. Those unique tracks are assigned a Track ID (B) which includes track information such as the number of spots, the track mean speed, track duration (and more). The yellow lines represent the region of interest drawn to only detect spots within the flow chamber. The magenta track (and magenta arrow) depicts a cell that is bound to the surface and the purple track (and purple arrow) depicts a cell that is rolling on the flow chamber floor because the 100-frame track projection is stationary and moving, respectively. The linking of spots to form tracks can be optimized in Trackmate, utilizing one of the several linking algorithms and optimization parameters. The inset is a zoom in on Track 8 where the 100-frame projected track is within the spot (or cell) radius indicating that the cell is not moving. (For interpretation of the references to colour in this figure legend, the reader is referred to the web version of this article.)

displacement, $D_{\max}$, and minimum time, $t_{\min}$. To evaluate if the tracks meet the stopping criteria, the RLNEK user must specify the minimum time, $t_{\min}$, that corresponds to biologically relevant non-specific binding time (defaulted at 0.2 s). The total number of tracks that meet the stopping criteria are the cumulative number of cell/spheres that bind to the ligand coated surface (i.e., N_b). For the tracks that satisfy the stopping criteria, the number of frames will be counted until the stopping criteria is broken. Each of these stopping events is converted to bond lifetime t_b, by frames per second, and arithmetically averaged over all stopping events. The dissociation rate, k_{off}, is the inverse of bond lifetime and is calculated for the given applied tensile force. The user can characterize $\frac{N_b}{N_T}$, and k_{off} over a range of applied tensile forces.

2.4.1. Evaluation of the bond dissociation model

After the user has tracked and characterized k_{off} at several physiologically relevant applied tensile forces, RLNEK will best-fit approximate the parameters of the slip and catch-slip bond dissociation models. The slip model is characterized by an exponential increase in k_{off} with increasing applied tensile force. The catch-slip model is characterized by, first, a decrease in k_{off} with increasing applied tensile force followed by an exponential increase in k_{off} with increasing applied tensile force. Simple linear regression and the Trust Region Reflective algorithm (TRR) (Branch et al., 1999) with a physical constraint of 0.01–10 nm on x_β are used for the slip and catch-slip models, respectively. The best-fit bond dissociation model is determined by evaluating the reactive compliance, x_β, after fitting. If the fitted x_β of the catch-slip bond

dissociation model is outside of the physical constraint range, then the slip bond dissociation model is selected. This physical constraint was determined by known receptor-ligand interactions (Cheung and Konstantopoulos, 2011) and has been validated for a set of T Cell Receptor interactions, published by (Liu et al., 2014), whereby RLNEK can distinguish between slip and catch-slip bond dissociation models (Fig. S1).

2.4.2. Single-molecule criteria

There are interpretation issues in claiming single-molecule interactions (Zhu et al., 2002) and measured interactions are likely for a small number of bonds; however, a module in RLNEK has been created to assess the single-molecule criteria. For a given applied tensile force, the distribution of bond lifetimes at different site densities and/or coating concentrations is compared with Welch's *t*-test. If the distributions of bond lifetime are not significantly different ($p > 0.05$), then the interactions are presumed to be single molecule over the corresponding site density/coating concentration range (Zhu et al., 2002).

2.5. Estimation of k_+

The interacting surfaces enclose a contact area, A_c, populated by a receptor site density, m_r. The effective on-rate is between the interacting surfaces and is defined as,

$$k_+ = A_c m_r k_{on} \tag{13}$$

The single molecule on-rate, k_{on}, includes the time scales of convective diffusion and reaction kinetics. Thus, $A_c k_{on}$ can be estimated utilizing the equation,

$$\frac{N_b}{N_T}(f) = \frac{m_r m_l A_c k_{on}}{m_r m_l A_c k_{on} + k_{off}(f)} \tag{14}$$

where the capture efficiency, $\frac{N_b}{N_T}$, and bond dissociation model, k_{off}, are calculated from collected and tracked video-microscopy data at several applied tensile forces. The ligand, m_l, and receptor, m_r, site-densities can be determined using several techniques such as fluorescent calibration (Chen et al., 2009), radiolabels (Dong et al., 2015), or atomic force microscopy (Blanchette et al., 2009; Cappuccio et al., 2008; Chuklanov et al., 2006). Thus, given site-densities and measurements of capture efficiency and bond lifetime as a function of applied tensile force, $A_c k_{on}$, and thus k_+, can be estimated at each applied tensile force.

is the cell/sphere radius and Ω is the rotational velocity. Approximating $\frac{d_c}{a} = 0.005$, hydrodynamic theory of motion of a sphere near a wall (Goldman et al., 1967) predicts the ratio $\frac{a\Omega}{u_{hd}} = 0.53$ and thus the relative surface velocity is estimated as $V = (1 - 0.53) * u_c$. The predicted ratio of rotational to hydrodynamic velocity, $\frac{a\Omega}{u_c}$, is interpolated based on user inputs of critical distance and cell/sphere radius, $\frac{d_c}{a}$. Receptor-ligand binding has been modelled as a two-step process where a receptor bound surface is traveling at a relative velocity to a ligand bound surface. For a binding event to occur, the receptor must first encounter the ligand (i.e., convective diffusion) and second react with the ligand (i.e., reaction kinetics).

The flux, J, of a receptor reaching a ligand within a reaction radius, α, for the first time can be solved utilizing the 2-D convective-diffusion equation. The dimensionless flux can be described as a Nusselt number $Nu = \frac{J}{\pi D m_l}$ and represented in terms of Pe by solving the convective-diffusion equation (Chang and Hammer, 1999),

$$Nu = 2\left[\frac{I_0\left(\frac{Pe}{2}\right)}{K_0\left(\frac{Pe}{2}\right)} + 2\sum_{n=1}^{\infty}(-1)^n \frac{I_n\left(\frac{Pe}{2}\right)}{K_n\left(\frac{Pe}{2}\right)}\right] \tag{16}$$

where I_n and K_n are modified Bessel functions of the second kind. The Nu is calculated by a 100-term summation. Due to the stochastic nature of receptor-ligand interactions, the probability, P, that an encounter will lead to a binding event must be defined. This probability is approximated by (Chang and Hammer, 1999),

$$P = \frac{k_{in}}{\left(k_{in} + \frac{1}{\varepsilon}\right)} \tag{17}$$

where ε is the average duration of encounter and k_{in} is the probability per unit time a receptor-ligand pair, within the reactive circle, will lead to a binding event. The intrinsic reaction rate, k_{in}, depends on the vibrational motion of the receptor and ligand and is treated as a constant. The encounter duration, represents the average time needed for a receptor to cross the boundaries of the ligand's reactive circle. Moreover, the probability of interaction reaches exactly zero if the timescale of the receptor traveling across the reaction distance of the ligand is less than the time of bond formation. The average encounter duration is determined by solving the Fokker-Planck equation and utilizing the first passage time approach (Chang and Hammer, 1999),

$$\varepsilon = \frac{a}{V}\left(\frac{-I_1\left(\frac{V\alpha^2}{2D}\right)^3}{I_0\left(\frac{V\alpha^2}{2D}\right)} + \sum_{n=1}^{\infty}(-1)^{n+1}\frac{I_{n-1}\left(\frac{V\alpha^2}{2D}\right)I_{n+1}\left(\frac{V\alpha^2}{2D}\right)\left(I_{n-1}\left(\frac{V\alpha^2}{2D}\right) + I_{n+1}\left(\frac{V\alpha^2}{2D}\right)\right)}{I_n\left(\frac{V\alpha^2}{2D}\right)}\right) \tag{18}$$

2.6. Estimation of k_{in}

The rate of receptor-ligand reactions bound to interacting surfaces is governed by the relative motion of the respective surfaces (Fig. 1C) and thus a Peclet number is defined to scale the relative surface velocity and the lateral receptor-ligand diffusivity (Chang and Hammer, 1999),

$$Pe = \frac{V\alpha}{D} \tag{15}$$

where V is the relative surface velocity, α is the reactive radius around the receptor, and D is the sum of the surface diffusivities $D = D_1 + D_2$ (Fig. 1C). The relative surface velocity is defined as $V = u_c - a\Omega$ where a

The perfect encounter rate constant is defined as $k_o = \pi D Nu = \frac{J}{m_l}$. Thus, the single molecule on rate is a function of only system parameters (Table 1, Table 2) and the relative surface velocity (19),

$$k_{on} = k_o P = \pi D Nu P \tag{19}$$

With the experimental measurements of $k_+(V)$ and the estimation of system parameters (i.e., D, α, d_c, m_r), the Nusselt number, $Nu(V)$, and encounter duration, $\varepsilon(V)$, can be calculated. Finally, the cell/sphere contact area and k_{in} are fit to Eqs. (17)–(20) by TRR nonlinear regression. Physical constraints are prescribed to A_c $(0, 4\pi r^2]$ and $k_{in}(0, \infty)$.

Table 1
Approximated system parameters.

Parameter	Value	Units	Definition	Reference
α	2	nm	Reactive Radius	(Caputo et al., 2007)
D	0.15	$\frac{\mu m^2}{s}$	Lateral Diffusivity	(Caputo et al., 2007)
d_c	25	nm	Critical cut-off distance	(Chang and Hammer, 1999)
μ	6.92×10^{-3}	$\frac{dyne*s}{cm^2}$	Fluid Viscosity	–
T	310	K	Temperature	–
k_b	1.38×10^{-23}	$\frac{J}{K}$	Boltzmann Constant	–

Table 2
Experimental system parameters.

a	μm	Cell/Sphere Radius
w	μm	Chamber Width
b	μm	Chamber Half-Height
L	nm	Receptor-Ligand Bond Length

These constraints assume the contact area, A_c, cannot exceed the surface area of the cell/sphere and that the probability of interaction, P, is between 0 and 1.

$$k_+ = A_c m_r k_{on} = A_c m_r k_o P = A_c m_r \pi DNuP \tag{20}$$

3. Assumptions and limitations

The theoretical foundation is built on analytical solutions and idealized assumptions that introduce parameter estimation error. The chamber floor is assumed atomically smooth and is only protruded by functionalized reactive ligands that do not disrupt the flow field. The cells/spheres enter the flow chamber and experience translational forces by gravity and convective motion. These forces cause the cells/spheres to translate along a trajectory and settle along the chamber floor (Munn et al., 1994; Zhang and Neelamegham, 2002). Observed cell/sphere tracks are assumed to be rolling along the flow chamber surface below a critical velocity, obtained from Eq. 4. Throughout the occurrence of a binding event, the cells/spheres are assumed unperturbed by upstream cells/spheres and the disrupted flow field downstream does not affect the downstream cells/spheres. Assumptions about flow field disruption can be optimized with control of inlet cell/sphere concentration. Cells are idealized as rigid spheres; however, at high hydrodynamic shear ($\gamma_w > 100\ s^{-1}$) the cell membrane can undergo viscoelastic deformation (Jadhav et al., 2005; Khismatullin and Truskey, 2012) likely reducing the estimated applied tensile force. Moreover, immune cells often have microvilli, with receptors concentrated at the tip (Designed Research; Y, 2016), that extend upwards of 1 μm from the surface (Majstoravich et al., 2004). This convolutes the critical interaction distance, d_c, and impedes the ability to accurately determine the interfacial contact area, A_c. Additionally, the tensile force is assumed to be applied on the trailing receptor-ligand interaction tethering the cell/sphere to the surface. This assumption is an idealization, and the applied tensile force is likely smaller in magnitude and a complex function of the shear rate, the dynamic interfacial contact area, and receptor-ligand site density. Although we provide a "single molecule" criteria module (*see User Guide*), due to the dynamic interfacial contact area/site density and unknown receptor-ligand interaction independence, the measured interactions are likely for a small number of bonds. Moreover, dissociation is modelled as one-step process where bonds break up simultaneously. A compilation of approximated parameters (Table 1) is implemented; however, these parameters can be readily interchanged to provide robust customizability.

4. Experimental methods

The data acquisition was used only to test and validate the functionality of the RLNEK software. Our group has significant experience in microfluidics (Bi et al., 2020; Glaser et al., 2021; Sewell-Loftin et al., 2020; Weng et al., 2020) and the laminar flow chamber device was manufactured using standard soft photolithography techniques previously described (Moya et al., 2013; Pan et al., 2017). Briefly, a master mold was created in a single mask photolithography step and this mold was used to curate a polydimethylsiloxane (PDMS) architecture. The PDMS architecture was then plasma bonded to a glass slide (Fisher Scientific). The microfluidic design was a singular channel with dimensions 10 mm × 0.8 mm × 0.1 mm (length x width x height). The flow chamber floor was functionalized with a target ligand utilizing a previously described Neutravidin™ -biotin based immobilization (Kim et al., 2009; Wang et al., 2012). Briefly, the flow chamber (already bonded to the glass slide) is plasma cleaned, incubated in silanization solution (3-MPS), washed with ethanol, incubated in GMBS, washed with ethanol, and incubated in Neutravidin™ solution. Utilizing this procedure, any target ligand that is biotinylated can be functionalized to the flow chamber surface and the coating concentration can be varied to control site density. Importantly, RLNEK is agnostic to the functionalization procedure and alternative linker chemistries may be used to functionalize a target ligand.

Video microscopy was performed on an IX83 inverted microscope (Olympus) and recorded with a 10× objective at 8 FPS. Tensile/tether force was controlled by varying the volumetric flow as described in Eq. 9. The flow in the microfluidic chamber was controlled by fastening plastic tubing to one end of the channel and coupling the tubing to a 5 mL syringe (BD Luer-Lok™). On the opposite end of the channel, the receptor-tethered cells/spheres were loaded into a pipette tip. The flow was precisely controlled by displacing the syringe's piston using a syringe pump apparatus (Harvard Apparatus PHD ULTRA™) in withdrawal mode.

Cell/sphere positions were tracked using Trackmate software (Tinevez et al., 2017) and the "tracks" and "spots" files are extracted for a given condition. For Trackmate, spots were detected by microscopically measuring cell diameters at 40× (i.e., 15.2 μm) and utilizing the built-in LoG spot detector (blob diameter = 15.2 μm and threshold = 0.30–0.50 μm). Next, the identified spots were filtered by setting a maximal intensity and linked between frames using the simple LAP tracer (maximum linking distance = 15 μm, maximum gap distance =15 μm, and maximum gap length = 10 frames). The linked frames are group into tracks, subscribed a Track ID, and filtered based on track duration. These Trackmate algorithms and parameters were implemented to demonstrate software utility, however, these will depend on the user setup (e.g., microscope, microscope settings, syringe pump, cell/sphere radius, flow rate). System parameters (Tables 1-2) and extracted files were used as inputs to RLNEK module.

A process flow diagram provides interpretability of the experimental data needed to obtain kinetic parameters of interest for a given receptor-ligand pair (Fig. S2). Please review the *User Guide* to identify the set of conditions that need to be collected to perform kinetic parameter calculations for each module. Moreover, there are several tuning parameters on the microscope including frames per second, brightness, exposure time, focal plane, cleaning of microscope slides, employing cell-dye, etc. We recommend starting the focal plane below the flow chamber and gradually increasing the focal plane until reaching cells/spheres on the flow chamber surface (before commencing volumetric flow). Then, maximize contrast between the cell and the background by adjusting microscope settings.

5. Discussion and availability

The analysis and equations provided above represent a compilation of contributions by numerous previous investigators and provides the

theoretical foundation to analytically assess receptor-ligand non-equilibrium kinetics from laminar flow chamber data. The functionality of the software has been partitioned into two predominant use cases (Fig. S2), both of which assume the user has obtained accurate, reproducible tracking optimization via Trackmate in ImageJ (see Trackmate guide on Github). The first use case does not require characterization of receptor or ligand site density and computes the capture efficiency, $\frac{N_b}{N_T}(f)$, and appropriate bond dissociation model, $k_{off}(f)$. The second use case requires receptor, m_r, and ligand, m_l, site densities. This use case additionally computes the effective on-rate, $k_+(f)$, single molecule on rate, $A_c k_{on}(f)$, and the intrinsic reaction rate, k_{in}. Detailed process flow diagrams and information on the required data to complete these calculations can be found in the *User Guide*. The software is written in the python environment utilizing several packages from the python standard library (i.e., operator, math, os, sys, warnings, csv) (Rossum and Drake, 2010). Trackmate output csv files are read into python with pandas (Mckinney, 2010). Scipy (Virtanen et al., 2020) and numpy (Harris et al., 2020) packages are used to perform mathematical operations (e.g., Bessel functions, curve fitting, etc.). Matplotlib (Hunter and Hunter, 2007) is used to graph results. Dependencies correspond with the relevant version of RLNEK. RLNEK 1.0, is an open, extensible software and future updates will include parallel compute acceleration, gpu acceleration, a graphic user interface, and the integration with Trackmate in ImageJ. The software is available for download at GitHub (https://github.com/zrollins/RLNEK). We have also provided Jupyter Notebooks for additional usability.

Supplementary data to this article can be found online at https://doi.org/10.1016/j.jim.2022.113381.

Declaration of Competing Interest

None.

Acknowledgements

This work was supported by the University of California, Davis, Department of Biomedical Engineering [startup funding to Steven C. George].

References

Alon, R., Hammer, D.A., Springer, T.A., 1995. Lifetime of the P-selectin-carbohydrate bond and its response to tensile force in hydrodynamic flow. Nature 377, 86. https://doi.org/10.1038/377086a0.

Bell, G.I., 1980. Theoretical models for the specific adhesion of cells to cells or to surfaces. Adv. Appl. Probab. 12, 566–567. https://doi.org/10.1017/s0001867800035254.

Bi, Y., Shirure, V.S., Liu, R., Cunningham, C., Ding, L., Meacham, J.M., Goedegebuure, S. P., George, S.C., Fields, R.C., 2020. Tumor-on-a-chip platform to interrogate the role of macrophages in tumor progression. Integr. Biol. 12, 221–232. https://doi.org/10.1093/INTBIO/ZYAA017.

Blanchette, C.D., Cappuccio, J.A., Kuhn, E.A., Segelke, B.W., Benner, W.H., Chromy, B. A., Coleman, M.A., Bench, G., Hoeprich, P.D., Sulchek, T.A., 2009. Atomic force microscopy differentiates discrete size distributions between membrane protein containing and empty nanolipoprotein particles. Biochim. Biophys. Acta Biomembr. 1788, 724–731. https://doi.org/10.1016/j.bbamem.2008.11.019.

Branch, M.A., Coleman, T.F., Li, Y., 1999. Subspace, interior, and conjugate gradient method for large-scale bound-constrained minimization problems. SIAM J. Sci. Comput. 21, 1–23. https://doi.org/10.1137/S1064827595289108.

Cappuccio, J.A., Blanchette, C.D., Sulchek, T.A., Arroyo, E.S., Kralj, J.M., Hinz, A.K., Kuhn, E.A., Chromy, B.A., Segelke, B.W., Rothschild, K.J., Fletcher, J.E., Katzen, F., Peterson, T.C., Kudlicki, W.A., Bench, G., Hoeprich, P.D., Coleman, M.A., 2008. Cell-free co-expression of functional membrane proteins and apolipoprotein, forming soluble nanolipoprotein particles. Mol. Cell. Proteomics 7, 2246–2253. https://doi.org/10.1074/mcp.M800191-MCP200.

Caputo, K.E., Lee, D., King, M.R., Hammer, D.A., 2007. Adhesive dynamics simulations of the shear threshold effect for leukocytes. Biophys. J. 92, 787–797. https://doi.org/10.1529/biophysj.106.082321.

Chang, K.C., Hammer, D.A., 1999. The forward rate of binding of surface-tethered reactants: effect of relative motion between two surfaces. Biophys. J. 76, 1280–1292. https://doi.org/10.1016/S0006-3495(99)77291-7.

Chen, Y., Munteanu, A.C., Huang, Y.F., Phillips, J., Zhu, Z., Mavros, M., Tan, W., 2009. Mapping receptor density on live cells by using fluorescence correlation spectroscopy. Chem. Eur. J. 15, 5327–5336. https://doi.org/10.1002/chem.200802305.

Cheung, L.S.L., Konstantopoulos, K., 2011. An analytical model for determining two-dimensional receptor-ligand kinetics. Biophys. J. 100, 2338–2346. https://doi.org/10.1016/j.bpj.2011.04.013.

Chuklanov, A.P., Ziganshina, S.A., Bukharaev, A.A., 2006. Computer program for the grain analysis of AFM images of nanoparticles placed on a rough surface. Surf. Interface Anal. 38, 679–681. https://doi.org/10.1002/sia.2294.

Designed Research; Y, G.H.J., 2016. Three-dimensional localization of T-cell receptors in relation to microvilli using a combination of superresolution microscopies. https://doi.org/10.1073/pnas.1605399113.

Dong, C., Liu, Z., Wang, F., 2015. Radioligand saturation binding for quantitative analysis of ligand-receptor interactions. Biophys. Reports 1, 148–155. https://doi.org/10.1007/s41048-016-0016-5.

Evans, E., Leung, A., Heinrich, V., Zhu, C., 2004. Mechanical switching and coupling between two dissociation pathways in a P-selectin adhesion bond. Proc. Natl. Acad. Sci. U. S. A. 101, 11281–11286. https://doi.org/10.1073/pnas.0401870101.

Glaser, D.E., Curtis, M.B., Sariano, P.A., Rollins, Z.A., Shergill, B.S., Anand, A., Deely, A. M., Shirure, V.S., Anderson, L., Lowen, J.M., Ng, N.R., Weilbaecher, K., Link, D.C., George, S.C., 2021. Biomaterials xxx (xxxx) xxx organ-on-a-chip model of vascularized human bone marrow niches. Biomaterials 121245. https://doi.org/10.1016/j.biomaterials.2021.121245.

Goldman, A.J., Cox, R.G., Brenner, H., 1967. Slow viscous motion of a sphere parallel to a plane wall-II Couette flow. Chem. Eng. Sci. 22, 653–660. https://doi.org/10.1016/0009-2509(67)80048-4.

Harris, C.R., Millman, K.J., van der Walt, S.J., Gommers, R., Virtanen, P., Cournapeau, D., Wieser, E., Taylor, J., Berg, S., Smith, N.J., Kern, R., Picus, M., Hoyer, S., van Kerkwijk, M.H., Brett, M., Haldane, A., del Río, J.F., Wiebe, M., Peterson, P., Gérard-Marchant, P., Sheppard, K., Reddy, T., Weckesser, W., Abbasi, H., Gohlke, C., Oliphant, T.E., 2020. Array programming with NumPy. Nature 5857825 (585), 357–362. https://doi.org/10.1038/s41586-020-2649-2.

Hunter, J.D., Hunter, D.J., 2007. Matplotlib: a 2D graphics environment. CSE 9, 90–95. https://doi.org/10.1109/MCSE.2007.55.

Jadhav, S., Eggleton, C.D., Konstantopoulos, K., 2005. A 3-D computational model predicts that cell deformation affects selectin-mediated leukocyte rolling. Biophys. J. 88, 96–104. https://doi.org/10.1529/biophysj.104.051029.

Khismatullin, D.B., Truskey, G.A., 2012. Leukocyte rolling on P-selectin: a three-dimensional numerical study of the effect of cytoplasmic viscosity. Biophys. J. 102, 1757–1766. https://doi.org/10.1016/j.bpj.2012.03.018.

Kim, Y.G., Moon, S., Kuritzkes, D.R., Demirci, U., 2009. Quantum dot-based HIV capture and imaging in a microfluidic channel. Biosens. Bioelectron. 25, 253–258. https://doi.org/10.1016/j.bios.2009.06.023.

Lawrence, M.B., Kansas, G.S., Kunkel, E.J., Ley, K., 1997. Threshold levels of fluid shear promote leukocyte adhesion through selectins (CD62L,P,E). J. Cell Biol. 136, 717–727. https://doi.org/10.1083/jcb.136.3.717.

Limozin, L., Bridge, M., Bongrand, P., Dushek, O., van der Merwe, P.A., Robert, P., 2019. TCR–pMHC kinetics under force in a cell-free system show no intrinsic catch bond, but a minimal encounter duration before binding. Proc. Natl. Acad. Sci. 201902141 https://doi.org/10.1073/pnas.1902141116.

Liu, B., Chen, W., Evavold, B.D., Zhu, C., 2014. Accumulation of dynamic catch bonds between TCR and agonist peptide-MHC triggers T cell signaling. Cell 157, 357–368. https://doi.org/10.1016/j.cell.2014.02.053.

Lou, J., Yago, T., Klopocki, A.G., Mehta, P., Chen, W., Zarnitsyna, V.I., Bovin, N.V., Zhu, C., McEver, R.P., 2006. Flow-enhanced adhesion regulated by a selectin interdomain hinge. J. Cell Biol. 174, 1107–1117. https://doi.org/10.1083/jcb.200606056.

Majstoravich, S., Zhang, J., Nicholson-Dykstra, S., Linder, S., Friedrich, W., Siminovitch, K.A., Higgs, H.N., 2004. Lymphocyte Microvilli Are Dynamic, Actin-Dependent Structures that Do Not Require Wiskott-Aldrich Syndrome Protein (WASp) for their Morphology. https://doi.org/10.1182/blood-2004-02-0437.

Mckinney, W., 2010. Data Structures for Statistical Computing in Python.

Moya, M., Tran, D., George, S.C., 2013. An integrated in vitro model of perfused tumor and cardiac tissue. Stem Cell Res Ther 4 (Suppl), 1. https://doi.org/10.1186/SCRT376.

Munn, L.L., Melder, R.J., Jain, R.K., 1994. Analysis of cell flux in the parallel plate flow chamber: implications for cell capture studies. Biophys. J. 67, 889–895. https://doi.org/10.1016/S0006-3495(94)80550-8.

Pan, H., Gray, R., Braybrooke, J., Davies, C., Taylor, C., McGale, P., Peto, R., Pritchard, K. I., Bergh, J., Dowsett, M., Hayes, D.F., 2017. 20-year risks of breast-Cancer recurrence after stopping endocrine therapy at 5 years. N. Engl. J. Med. 377, 1836–1846. https://doi.org/10.1056/NEJMOA1701830/SUPPL_FILE/NEJMOA1701830_DISCLOSURES.PDF.

Pierres, A., Benoliel, A.M., Bongrand, P., 1995. Measuring the lifetime of bonds made between surface-linked molecules. J. Biol. Chem. https://doi.org/10.1074/jbc.270.44.26586.

Robert, P., Aleksic, M., Dushek, O., Cerundolo, V., Bongrand, P., Van Der Merwe, P.A., 2012. Kinetics and mechanics of two-dimensional interactions between T cell receptors and different activating ligands. Biophys. J. 102, 248–257. https://doi.org/10.1016/j.bpj.2011.11.4018.

Rossum, G., Drake, F.L., 2010. The Python Library Reference. October 1–1144.

Sewell-Loftin, M.K., Katz, J.B., George, S.C., Longmore, G.D., 2020. Micro-strains in the extracellular matrix induce angiogenesis. Lab Chip 20, 2776–2787. https://doi.org/10.1039/D0LC00145G.

Shirure, V.S., Liu, T., Delgadillo, L.F., Cuckler, C.M., Tees, D.F.J., Benencia, F., Goetz, D. J., Burdick, M.M., 2015. CD44 variant isoforms expressed by breast cancer cells are

functional E-selectin ligands under flow conditions. Am. J. Physiol. Physiol. 308, C68–C78. https://doi.org/10.1152/ajpcell.00094.2014.

Tinevez, J.Y., Perry, N., Schindelin, J., Hoopes, G.M., Reynolds, G.D., Laplantine, E., Bednarek, S.Y., Shorte, S.L., Eliceiri, K.W., 2017. TrackMate: an open and extensible platform for single-particle tracking. Methods 115, 80–90. https://doi.org/10.1016/j.ymeth.2016.09.016.

Virtanen, P., Gommers, R., Oliphant, T.E., Haberland, M., Reddy, T., Cournapeau, D., Burovski, E., Peterson, P., Weckesser, W., Bright, J., van der Walt, S.J., Brett, M., Wilson, J., Millman, K.J., Mayorov, N., Nelson, A.R.J., Jones, E., Kern, R., Larson, E., Carey, C.J., Polat, I., Feng, Y., Moore, E.W., VanderPlas, J., Laxalde, D., Perktold, J., Cimrman, R., Henriksen, I., Quintero, E.A., Harris, C.R., Archibald, A.M., Ribeiro, A. H., Pedregosa, F., van Mulbregt, P., 2020. SciPy 1.0: fundamental algorithms for scientific computing in Python. Nat. Methods 173 (17), 261–272. https://doi.org/10.1038/s41592-019-0686-2.

Wang, S., Esfahani, M., Gurkan, U.A., Inci, F., Kuritzkes, D.R., Demirci, U., 2012. Efficient on-chip isolation of HIV subtypes. Lab Chip 12, 1508–1515. https://doi.org/10.1039/c2lc20706k.

Weng, K.C., Kurokawa, Y.K., Hajek, B.S., Paladin, J.A., Shirure, V.S., George, S.C., . Human Induced Pluripotent Stem-Cardiac-Endothelial-Tumor-on-a-Chip to Assess Anticancer Efficacy and Cardiotoxicity. https://home.liebertpub.com/tec, 26, pp. 44–55. https://doi.org/10.1089/TEN.TEC.2019.0248.

Zhang, Y., Neelamegham, S., 2002. Estimating the efficiency of cell capture and arrest in flow chambers: study of neutrophil binding via E-selectin and ICAM-1. Biophys. J. 83, 1934–1952. https://doi.org/10.1016/S0006-3495(02)73956-8.

Zhu, C., Long, M., Chesla, S.E., Bongrand, P., 2002. Measuring receptor/ligand interaction at the single-bond level: experimental and interpretative issues. Ann. Biomed. Eng. 30, 305–314. https://doi.org/10.1114/1.1467923.